Journal of Catalysis **209,** 62–68 (2002)
doi:10.1006/jcat.2002.3621

Active Morphology of Au/γ-Al_2O_3—A Model by EXAFS

C.-H. Lin, S.-H. Hsu, M.-Y. Lee, and S. D. Lin[1]

Department of Chemical Engineering, Yuan Ze University, Chung-Li, Taiwan 320, Republic of China

Received September 24, 2001; revised March 19, 2002; accepted March 19, 2002

Au/γ-Al_2O_3 catalysts were prepared by depositing $AuCl_3$ onto low-soda γ-Al_2O_3 under different pH. EXAFS (extended X-ray absorption fine structure) analysis showed that Au species were mainly in the Au–O bonding environment when dried at 298 K, regardless of the suspension pH during deposition. Au–(O)–Al bonding was also suggested from EXAFS analysis of catalysts prepared at pH ranging from 4.1 to 9.4, indicating a deposition via the coordination of surface hydroxyl groups to Au species. However, Au–(O)–Au was found instead of Au–(O)–Al in the catalyst prepared at an extreme pH of 10.5, indicating a deposition of polymeric $Au(OH)_3$. The catalysts were tested for CO oxidation without further pretreatment. The one prepared at pH 10.5 catalyzed the CO oxidation reaction effectively at 323 K whereas that prepared at pH 4.1 showed negligible activity. This suggested that a specific Au–O morphology, such as the polymeric $Au(OH)_3$, could be responsible for the high CO oxidation activity of supported Au catalysts.

Key Words: **Au catalysts; Al_2O_3; CO oxidation; EXAFS; pH effect; deposition.**

1. INTRODUCTION

Supported gold catalysts are very active in catalyzing many types of reactions. Gold particles smaller than 5 nm, in addition to low chlorine residue, are considered essential for the high activity (1–5). As a consequence, catalyst preparation becomes critical to good catalysis. The pioneering work by Haruta and co-workers (1) used a coprecipitation method to prepare Au catalysts. Later on, a deposition method (2) emerged to overcome the high-Au-loading problem in the coprecipitation method. It is the most common method used in the literature, although impregnation and the vapor deposition method can also be found. This most popular deposition procedure involves the pH adjustment of Au precursor solution and the addition of support afterward (2). This is similar to the preparation of Au sol (6) followed by its deposition on the support. However, there is a different deposition procedure used for Group VIII metal catalysts which involves the pH adjustment of support suspension followed by the addition of metal precursor. Although Chen and Yeh (7) recently reported that both procedures can produce active supported Au catalysts, this study explored the role of suspension pH on the Au catalysts prepared by the latter deposition procedure.

The origins of the high activities of supported Au catalsyts are discussed in the literature. A model attributing the enhanced CO oxidation activity to a synergistic effect in the Au–oxide interfacial regions (2–5, 8–10) seems to be better accepted. Among various supports, reducible oxides such as TiO_2 are more popular because they produce Au catalysts with high activities and, from past experience with strong metal–support interaction (SMSI) phenomena, they are expected to follow the synergistic Au–oxide interfacial site model. However, refractory oxides are also efficient enough to prepare good Au catalysts (7), but the origin of the synergistic Au–oxide interfacial site is not as obvious as that of the Au supported on reducible oxides. A careful study of the active Au supported on refractory oxides could help to explain the active morphology of Au catalysts. Therefore, this study used γ-Al_2O_3 as the support for Au catalysts. Extended X-ray absorption fine structure (EXAFS) spectroscopy was used to examine the Au morphology following the less commonly used deposition preparation of Au/γ-Al_2O_3 catalysts. The Au morphology as affected by the preparation parameters is reported and the possible deposition mechanisms and the structure of active sites are discussed.

2. EXPERIMENTAL

$AuCl_3$ (Aldrich, 64.9% Au) was deposited on γ-Al_2O_3 (Strem, 99%, low soda, 80–120 mesh, precalcined at 823 K for 1 h) to make 1% Au/γ-Al_2O_3. One gram of Al_2O_3 was dispersed in 50 ml of deionized water and the pH of the Al_2O_3 suspension was adjusted by adding 1 M NH_4OH (diluted from a 25% Merck solution). Thereafter, a solution of $AuCl_3$ in 10 ml of deionized water was added dropwise under magnetic stirring. After another hour of stirring and one more hour of aging, the solid was filtered and dried under rough vacuum at room temperature. The filtrate was metered and analyzed for Cl and Au content using ICP–MS

[1] To whom correspondence should be addressed. E-mail: sdlin@saturn.yzu.edu.tw.

0021-9517/02 $35.00

(Perkin–Elmer, SCIEX5000). Four catalysts were prepared under different pH conditions and are coded according to stabilized pH at 4.1, 8.4, 9.3, and 10.5, respectively. For the pH 4.1 sample, no alkaline was added to the Al_2O_3 suspension. It has an initial pH of around 7 but drops and stabilizes at 4.1 after the addition of $AuCl_3$ solution. For the other three catalysts, alkali was added until reaching the target pH of 8.5, 9.5, and 10.5, respectively. The subsequent addition of $AuCl_3$ solution caused only minor changes in pH reading.

EXAFS experiments were performed at the Synchrotron Radiation Research Center (SRRC) in Taiwan with a storage ring energy of 1.5 GeV and a beam current between 150 and 200 mA. The Au L_{III} edge absorbance of powder catalysts was measured in transmission geometry at room temperature. The energy was scanned from 200 eV below to 1200 eV above the Au L_{III} edge (11,919 eV). EXAFS data analysis was carried out using University of Washington analysis programs. Radial distribution functions were obtained by Fourier-transformed k^3-weighted χ function. Detailed analysis was carried out by fitting the EXAFS data in a k range from 3 to 16 $Å^{-1}$ using a Hanning Window Fraction of 0.1. This fitting was performed against selective combination of the following coordination shells: Au–O, Au–Cl, Au–Au, Au . . . Au, and Au . . . Al. All these reference shells were obtained by theoretical calculation of the specific atom pair using Feff 7.02. The Au . . . Au shell was initiated to identify oligomerized $Au(OH)_xCl_y$ species where a bridging atom (e.g., Cl or O) in between two Au atoms was assumed with a structure like that of Au_2Cl_6 (11) and of Au_2O_3 (12). The Au . . . Al coordination was initiated to identify, if any, adsorbed Au species via surface hydroxyl groups. Thus, an Au–O–Al bonding environment is assumed initially and its bond distance was estimated based on standard Au–O and Al–O bond distances. $AuCl_3$ (Aldrich) and $Au(OH)_3$ (Aldrich) are tested similarly for comparison purpose.

Diffuse-reflectance UV/visible spectroscopy (DRS) was conducted with a commercial unit (Hitachi, U-3410, with 150 ϕ integrating sphere) over air-exposed catalyst powders. The scan was made at 60 nm/min from 800 to 185 nm with a band pass of 2 nm.

CO oxidation was conducted at 1% CO + 10% O_2 (balanced with He) using a flow-type packed-bed microreactor system operated at 1 atm. The CO space velocity was kept at 71.4 μmol/min/g of cat. Both CO (San-Fu, 4% CO in He) and oxygen (San-Fu, 99.8%) streams were treated with an online moisture trap (Alltech). He (San-Fu, 99.995%) carrier was further treated with an Oxytrap (Alltech). Mass flow controllers (Tylan) were used to control the flow rates. The reactor effluent was analyzed using a GC (Varian, 3300) in line via a six-port valve (Valco), with a Porapak®Q-Porapak®R-series packed column and a thermal conductivity detector. The mass balance of the effluents was typically within ±10% of the feed.

3. RESULTS

Procedures used in this study successfully deposited 1% Au onto γ-Al_2O_3 within a suspension pH range from 4.1 to 10.5. Table 1 lists the measured Au loading and Cl residue based on the ICP–MS analysis of filtrates from the deposition preparation. Chlorine residue decreased when the suspension pH was increased. This Cl residue is expected to correlate with the chemical identities of liquid-phase species during catalyst preparation. $AuCl_3$ aqueous solution may contain $[AuCl_n(OH)_{4-n}]^-$ ions ($n = 1, 2, 3, 4$), and neutral $AuCl_3$ and $Au(OH)_3$. The species distribution depends on solution pH. $Au(OH)_3$ and $Au(OH)_4^-$ appear to be the dominating species within a pH range from 7 to 10, while a solution of pH 4.1 may contain both $[AuCl_2(OH)_2]^-$ and $[AuCl_3(OH)]^-$ ions (13, 14). This can qualitatively explain the Cl/Au ratio for the pH 4.1 sample but it conflicts with that of the Au/γ-Al_2O_3 prepared at pH 8.6 shown in Table 1. The other factor that can affect the adspecies structure is the surface charge. The positively charged Al_2O_3 surface at pH 4.1 can readily adsorb anions. Consequently Au anions and Cl^- in liquid phase will compete for adsorption sites and it is not surprising that the Cl residue could reach a Cl/Au ratio of 2.3. On the other hand, a low Cl residue is expected at a pH range of 8–10.5 since $Au(OH)_3$ and $[Au(OH)_4]^-$ are the major Au aqueous species. However, the negatively charged surface should not adsorb Cl^- as well as Au anions. In order to account for effective loading of Au, the deposition should occur via the precipitation of neutral $Au(OH)_xCl_y$ oligomers or the coordination of surface groups as the ligands of Au anions. A decreasing Cl residue from pH 8.5–10.5 (see Table 1) is considered to reflect the decreasing Cl content in such deposit.

Figure 1 shows the radial distribution function obtained from EXAFS measurements of Au/γ-Al_2O_3 prepared at different pH. Au–O coordination is obviously the preferred morphology. It should be emphasized that these catalysts were filtered without washing, dried at 298 K under low vacuum, and then analyzed. Chemical identities of surface species are expected to be least disturbed from adspecies. The almost negligible Au–Cl coordination in any catalyst in Fig. 1 suggests that Cl residue came from independently

TABLE 1

Composition of Au/γ-Al_2O_3 Catalysts Prepared by Deposition at Different pH Values

pH	Au (wt%)[a]	Cl (wt%)[a]	Au/Cl (molar ratio)
4.1	1.1	0.45	2.3
8.6	1.1	0.43	2.3
9.4	1.0	0.24	1.3
10.5	1.0	Nil	Nil

[a] Calculated based on filtrate analysis with ICP–MS.

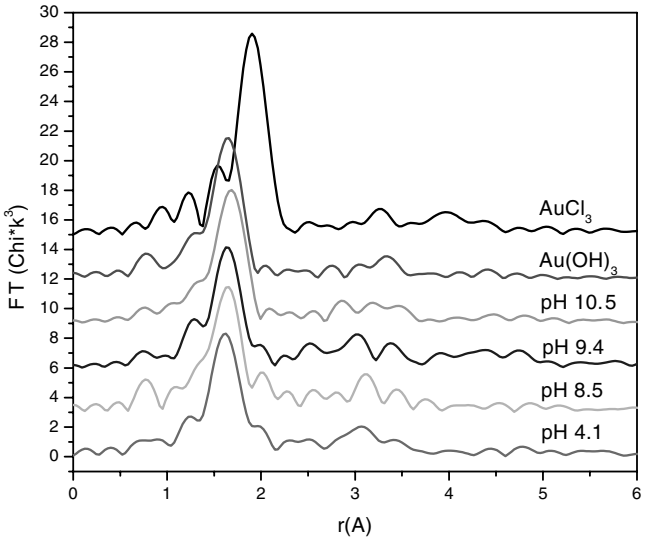

FIG. 1. Radial distribution function from X-ray absorption measurement of $AuCl_3$, $Au(OH)_3$, and $Au/\gamma\text{-}Al_2O_3$ prepared by deposition at a pH of 4.1, 8.5, 9.4, and 10.5. No phase correction was made.

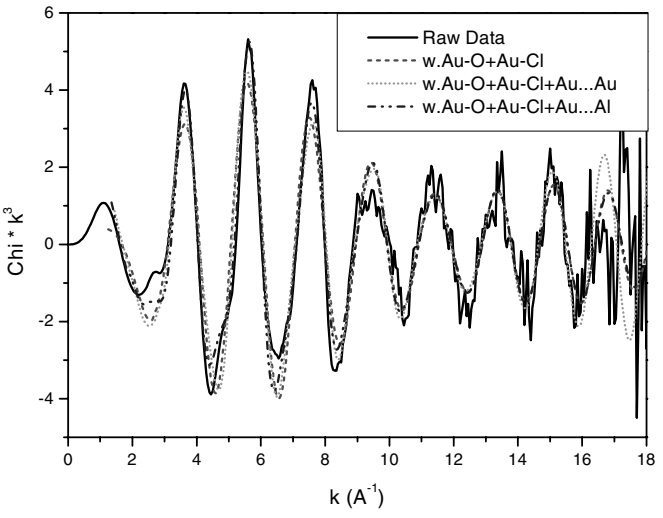

FIG. 2. Comparison of the k-space EXAFS data of $Au/\gamma\text{-}Al_2O_3$ (pH 4.1) against fitting with [Au–O + Au–Cl] (dashed line), [Au–O + Au–Cl + Au . . . Au] (dotted line), and [Au–O + Au–Cl + Au . . . Al] (dash–dot–dot line).

adsorbed Cl^- instead of the Cl ligand in Au adspecies. In addition, the surface hydroxyl groups might coordinate in substitute for Cl ligand to the deposited Au species in order to account for the negligible Au–Cl coordination for the pH 4.1 sample.

Table 2 lists the results of EXAFS detailed analysis. From Fig. 1, catalysts prepared at different pH have a similar Au–O main shell and minor differences, if any, at $r > 2.2$ Å. To show how the results of detailed analyses were obtained, Figs. 2 and 3 compare the fitting results of the catalyst prepared at pH 4.1 with respect to the raw data in k-space and to the Fourier-transformed data in r-space, respectively. Similarly, Figs. 4 and 5 show the fitting results of the catalyst prepared at pH 10.5 in k- and r-space, respectively. Comparing Figs. 2 and 4, the difference in k-space oscillation between the catalysts prepared at pH 4.1 and 10.5 can be found. The difference can be explained by the model fitting in Table 2.

TABLE 2

Results of Detailed EXAFS Analysis of $Au/\gamma\text{-}Al_2O_3$ Prepared by Deposition at Different pH Values

Sample	Shell	R (Å)	CN[a]	2	E_o (eV)
Au/Al_2O_3 (pH 4.1)	Au–O	1.987 ± 0.017	2.83 ± 0.76	0.003 ± 0.001	6.5 ± 1.9
	Au–Cl	2.255 ± 0.028	0.28 ± 0.45	0.001 ± 0.006	
	Au . . . Al	3.495 ± 0.035	5.30 ± 3.03	0.017 ± 0.008	
Au/Al_2O_3 (pH 4.1, washed)	Au–O	1.983 ± 0.004	3.18 ± 0.22	0.002 ± 0.003	8.8 ± 2.3
	Au . . . Al	3.487 ± 0.020	4.81 ± 2.13	0.014 ± 0.005	
Au/Al_2O_3 (pH 8.5)	Au–O	1.999 ± 0.009	3.87 ± 0.53	0.006 ± 0.001	8.2 ± 1.6
	Au–Cl	2.293 ± 0.011	0.01 ± 0.03	−0.009 ± 0.006	
	Au . . . Al	3.509 ± 0.033	4.87 ± 2.99	0.016 ± 0.008	
Au/Al_2O_3 (pH 9.4)	Au–O	2.003 ± 0.017	2.97 ± 0.89	0.003 ± 0.002	6.9 ± 2.2
	Au–Cl	2.265 ± 0.036	0.06 ± 0.24	−0.004 ± 0.012	
	Au . . . Al	3.535 ± 0.046	5.46 ± 6.43	0.017 ± 0.019	
	Au . . . Au	3.226 ± 0.030	0.58 ± 1.67	0.005 ± 0.009	
Au/Al_2O_3 (pH 10.5)	Au–O	2.016 ± 0.006	3.12 ± 0.30	0.003 ± 0.001	8.7 ± 1.3
	Au . . . Au	3.109 ± 0.018	1.45 ± 1.10	0.008 ± 0.004	
Au/Al_2O_3 (pH 10.5)	Au–O	2.017 ± 0.007	3.11 ± 0.34	0.003 ± 0.001	8.9 ± 1.5
	Au . . . Au	3.125 ± 0.050	1.32 ± 1.78	0.008 ± 0.008	
	Au . . . Al	3.221 ± 0.089	0.02 ± 0.18	−0.008 ± 0.027	
Au foil	Au–Au	2.862 ± 0.003	11.4 ± 0.6	0.008 ± 0.002	1.3 ± 0.6
$Au(OH)_3$	Au–O	1.991 ± 0.006	3.35 ± 0.30	0.003 ± 0.001	7.4 ± 1.3
$AuCl_3$	Au–Cl	2.273 ± 0.007	3.10 ± 0.43	0.004 ± 0.001	5.7 ± 1.3

[a] CN, Coordination number calculated from the amplitude ratio by assuming that CN/amplitude = 1.

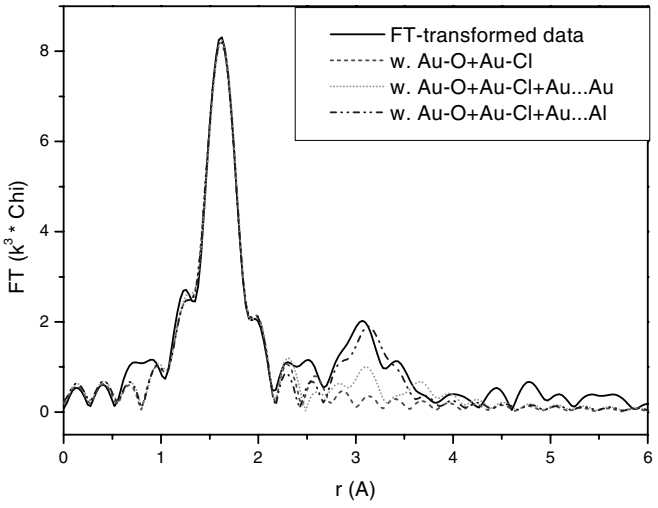

FIG. 3. Comparison of the Fourier-transformed EXAFS data of Au/γ-Al_2O_3 (pH 4.1) against fitting with [Au–O + Au–Cl] (dashed line), [Au–O + Au–Cl + Au . . . Au] (dotted line), and [Au–O + Au–Cl + Au . . . Al] (dash–dot–dot line).

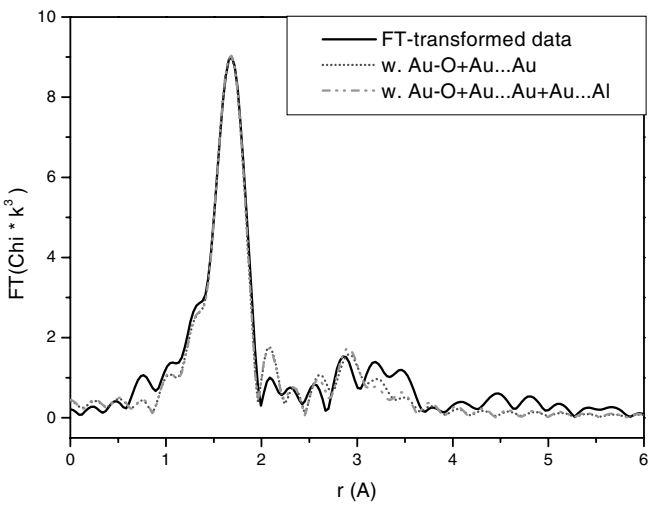

FIG. 5. Comparison of the Fourier-transformed EXAFS data of Au/γ-Al_2O_3 (pH 10.5) against fitting with [Au–O + Au . . . Au] (dotted line) and [Au–O + Au . . . Au + Au . . . Al] (dash–dot–dot line).

Results in Table 2 show that deposited $Au(OH)_xCl_y$ surface species have a first-shell coordination number of 3 ± 0.2, except the one deposited at pH 8.5. $AuCl_3$ (11) and other Au(III) compounds are reported to have Au^{+3} at a plane center having four coordination neighbors. However, EXAFS analyses on the fresh Au/γ-Al_2O_3 showed a total of ca. three first-shell coordination neighbors. The presence of a novel Au coordination geometry is considered unlikely because reference compounds, i.e., $Au(OH)_3$ and $AuCl_3$, also showed three first-shell neighbors in our experiments. The possible reasons for this odd coordination number include the fact that (i) the estimated coordination number may be subjected to some extent of uncertainty, and (ii) EXAFS may not reveal the presence of the neighbor having only weak interactions. From the literature (11), the fourth coordination in $AuCl_3$ is owing to the interaction between the lone-pair electron of Cl and the empty orbital of Au. This coordination may not be strong enough to cause a backscattered EXAFS signal. This may also explain the coordination number we observed in the $AuCl_3$ EXAFS experiment.

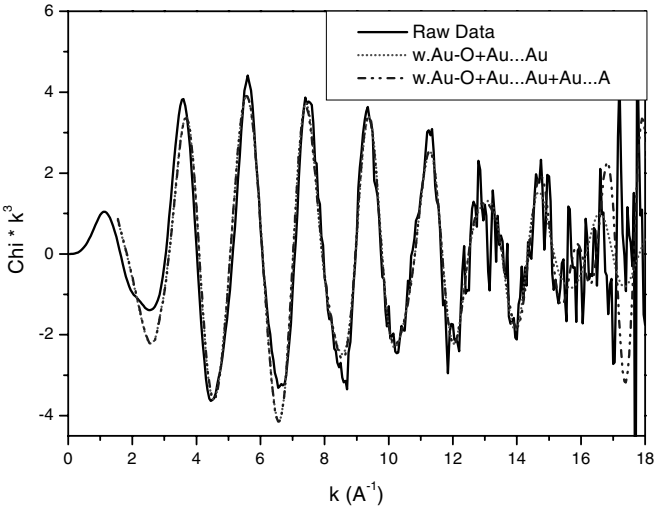

FIG. 4. Comparison of the k-space EXAFS data of Au/γ-Al_2O_3 (pH 10.5) against fitting with [Au–O + Au . . . Au] (dotted line) and [Au–O + Au . . . Au + Au . . . Al] (dash–dot–dot line).

From Table 2 it can be seen that Au–O is the major shell while Au–Cl is relatively minor and seems to present only at lower pH. This suggests that $Au(OH)_3$-like surface species present in the dried catalysts. This is similar to that proposed for $Au/Mg(OH)_2$ prepared by a different deposition procedure after a 353-K calcination in air (15). This indicates that different deposition procedures may lead to similar Au morphology and similar activity (7).

The presence of Au . . . Al shell, which has a bond distance slightly shorter than the sum of Au–O (1.98 Å for Au–OH (16)) and O–Al (1.6 Å in Al_2O_3 (17)), can be found in catalysts prepared at pH from 4.1 to 9.4. Their similar Au . . . Al coordination number indicates that surface hydroxyl groups act as coordination ligands in the $Au(OH)_3$-like deposit species. The presence of this Au . . . Al shell also indicates that Au–Al_2O_3 interaction occurs when the deposition takes place at lower pH.

This Au . . . Al shell diminishes when pH is raised to 10.5. This can be confirmed from the two sets of fitting results listed for Au/γ-Al_2O_3 at pH 10.5 in Table 2. Instead of the Au . . . Al shell, a second Au . . . Au shell appears in Au/γ-Al_2O_3 prepared at pH 10.5 (and 9.4). The bond distance of this Au . . . Au shell is close to an Au–O–Au configuration with Au–O = 2.0 Å and $\angle AuOAu \approx 104^\circ$, similar to the

structure of Au_2O_3 (12). Since the coordination number of the Au–O shell in this sample is 3 while that in Au_2O_3 is 4 (12, 18), it seems to be a deposition via the precipitation of $Au(OH)_3$ oligomers (or like $Au_2O_6^{-6}$ (19)). This species will be referred to as "polymeric $Au(OH)_3$" hereafter, since it is most likely from the aqueous $Au(OH)_3$ species. The gradual increase in Au–O bond distance from pH 4.1–10.5 shown in Table 2 also supports the shift of the deposit structure from one to the other. The Au–O bond distance of 1.987 Å for the pH 4.1 sample is consistent with that of Au–OH at 1.98 Å in $Au_2Sr(OH)_8$ (16) and a bond distance of 2.016 Å for the pH 10.5 sample is close to that of 2.01 Å in Au_2O_3 (12).

That there is no metallic Au deposit in the catalysts prepared at all pH values in this study is supported by the DRS measurement shown in Fig. 6. The presence of metallic Au can be characterized by a surface plasmom resonance peak around 500 nm (20), which cannot be found in Fig. 6. The absorbance peaks at 220–350 nm belongs to the ligand-to-metal charge transfer or ligand field (21). The somewhat different peak shape around 220–350 nm for the catalyst prepared at pH 10.5 seems to partially support the EXAFS analysis results. That is, the Au coordination environment in the catalyst prepared at pH 10.5 is different from that in catalysts prepared at lower pH (4.1–9.5).

CO oxidation over the two catalysts prepared at pH 4.1 and 10.5 showed very different activities. Figure 7 compares the CO conversion after ca. 1 h onstream at every test temperature in a sequential temperature-ascending experiment. The one prepared at pH 10.5 had a lighting-off temperature around 323 K, whereas the one prepared at pH 4.1 showed little activity at the same temperature. It should be noted that the catalysts were tested for CO oxidation without pretreatment; only He purging for more than 30 min at 298 K was carried out prior to the test. This indicates that the Au morphology of Au/Al_2O_3 prepared at pH 10.5 gives rise to a higher activity than that prepared at pH 4.1. This reveals that the polymeric $Au(OH)_3$ is or leads to the active morphology while the anchored $Au(OH)_3$-like deposit at lower pH is not. It should be noted that both morphologies have similar Au–O nearest shells but different second shells in EXAFS. This suggests the important contribution of the higher shells in supported Au catalysts.

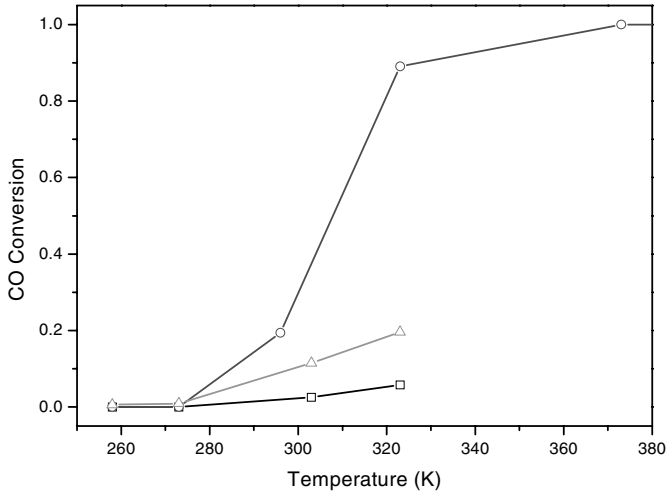

FIG. 7. CO oxidation over Au/γ-Al_2O_3 prepared by deposition at a pH of 4.1 (□) and 10.5 (○), and that of pH 4.1 after H_2O washing (△). The reaction was carried out at 1% CO + 10% O_2 (in He) and a space velocity of 71.4 mol/min/g of cat.

Figure 7 also elucidates the effect of washing on the pH 4.1 sample for CO oxidation. The catalytic activity was slightly enhanced but no obvious lighting-off was found as with the pH 10.5 sample. A washing procedure is typically associated with Au catalysts prepared by either coprecipitation or deposition (1, 2) in order to remove residual Cl. The EXAFS-resolved structure of this washed sample, shown in Table 2, confirms the removal of trace Au–Cl coordination, with the other coordination shells slightly altered. This reinforces the previous observation that the surface-anchored $Au(OH)_3$-like species (with an Au–O–Al coordination shell) is less active.

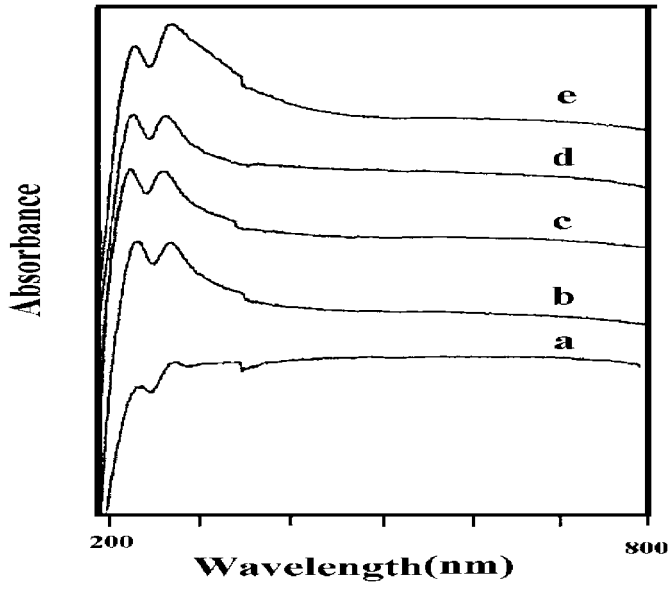

FIG. 6. Diffuse reflectance spectroscopy of γ-Al_2O_3 (a), and Au/γ-Al_2O_3 prepared by deposition at a pH of 4.1 (b), 8.5 (c), 9.4 (d), and 10.5 (e).

4. DISCUSSION

This study tried to screen artifacts in the prepared catalysts. A low-soda γ-Al_2O_3 was used and non-Na alkali was used for pH adjustment, although the effect of Na on supported Au catalysts was not discussed in the literature. In addition, the filtered catalyst powders were mostly not washed and a drying at room temperature was performed. Even the CO oxidation test was carried out without any

pretreatment (except He purge) on these catalysts and the reaction temperature was no higher than 323 K. This was to keep the Au deposit as undisturbed as possible. From catalysts following this procedure, EXAFS analysis showed that the structure of the Au deposit depended on the pH during Au deposition. An $Au(OH)_3$-like species anchored to surface via the coordination of surface hydroxyl groups was found at lower pH. This attribution is due to the observation of the Au–(O)–Al coordination and a Au–O coordination number of 3. Chlorine residue at lower pH was more likely a consequence of chloride ion adsorption. The Au deposit became polymeric $Au(OH)_3$ as the pH was raised to above 9. This attribution is due to the presence of a new Au–(O)–Au shell as the Au–(O)–Al disappeared. The Au–O coordination number was not changed at high pH. The CO activity test showed that the anchored $Au(OH)_3$-like deposit is much less active than the polymeric $Au(OH)_3$ deposit. This indicates that the polymeric $Au(OH)_3$ structure is or leads to the active morphology for CO oxidation at low temperature.

The presence of special metal–oxide interfacial sites has been adopted to explain the high activities of Au catalysts. Haruta and co-workers suggested that the reaction occurs between the CO on Au and the adsorbed oxygen anion on oxide (2). Bollinger and Vannice (9) used TiO_2-covered Au powders to demonstrate the significant activity enhancement from such interfacial regions. Grunwaldt and Baiker (10) discussed the role of oxygen vacancies on TiO_2. All these and many others proposed a synergistic effect between Au and "active" supports, as described recently by Schubert *et al.* (22). In this study, the presence of oxygen vacancies or the adsorbed oxygen on γ-Al_2O_3 is questionable. A partially dissolved γ-Al_2O_3 surface at pH as high as 10.5 may be the only possibility, but it is not strong enough to make a statement on the presence of the interfacial synergistic effect. This suggests that the polymeric $Au(OH)_3$ morphology can be active by itself or can be changed to the active morphology under the reaction environment used in this study.

Hydrated Au oxyhydroxide ($AuOOH \cdot xH_2O$) was identified in Au–Fe coprecipitated catalysts based on an empirical correlation of isomer shift and quadrupole splitting parameters in Mössbauer spectra (23, 24) and was attributed as the active phase (24). This oxyhydroxide identity may not be an exact active structure as is the polymeric $Au(OH)_3$ in this study; however, both structures indicate the involvement of certain Au–O bonding in the active phases of supported Au catalysts. Stangland *et al.* reported that the $Au(OH)_3$ and TiO_2-modified $Au(OH)_3$ can be active for selective partial oxidation of propylene (25). Au oxyhydroxide phase was considered to occur from the reduction or dehydration of $Au(OH)_3$ (25, 26). Though the mentioned literature and this study attribute oxidic Au as the active morphology in supported Au catalysts, it is important to note that not all oxidic Au works. From the results of this study, only certain specific structures, such as the polymeric $Au(OH)_3$, will become active.

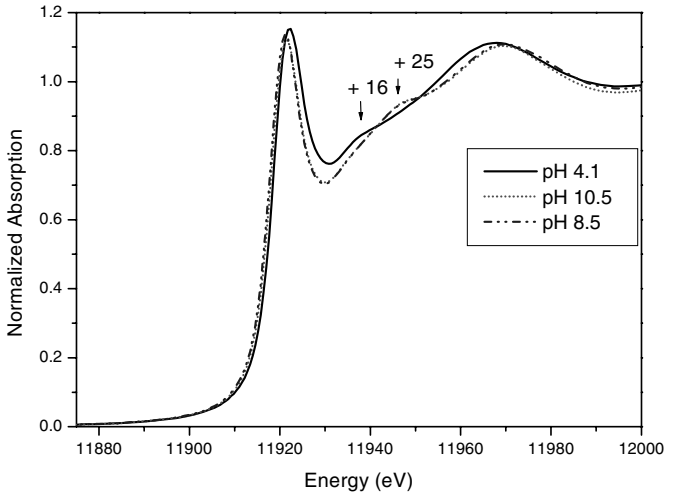

FIG. 8. XANES of Au/γ-Al_2O_3 prepared by deposition at a pH of 4.1, 8.5, and 10.5. The +16 and +25 eV resonances are relative to the whiteline position.

It is not clear from the results of this study whether it is the geometric or electronic structure or both that affects the activity of these Au–O sites. The Au–O morphology resolved for the Au/γ-Al_2O_3 prepared at pH 4.1 is not active for CO oxidation at 323 K. The presence of Au . . . Al coordination while having a low activity affirms that Al_2O_3 is an inert support. Figure 8 shows the XANES of Au/γ-Al_2O_3 prepared at pH 4.1, 8.5, and 10.3. The somewhat higher whiteline intensity of the pH 4.1 sample suggests a slightly lower electron density in its d-orbital. Two resonance features, at +16 and +25 eV, above the whiteline can be observed, respectively, in pH 4.1 and higher pH samples. Farges *et al.* reported the presence of +12 and +25 eV resonance features in aqueous $Au(OH)_xCl_y$ species (27). The +12 resonance decreased while the +25 resonance increased with increasing pH in their study. The +16 and +25 features in Fig. 8 show the same trend with pH. Farges *et al.* attributed the +12 resonance to multiple-scattering effects associated with 4-coordinated Au^{+3} and the +25 resonance to the presence of O (or OH, H_2O) around Au^{+3}, like that in Au_2O_3 or AuO_4^{-6} (27). These attributions are somewhat inconsistent with our results because none of our samples is without O coordination. It may be possible that the +16 and +25 resonances are associated with isolated and polymeric $Au^{+3}(OH)_3$ species, respectively. Considering the geometry effect, both the inactive and active Au–O morphology have a similar coordination number. However, the less active Au–O morphology has a shorter bond distance than the active morphology. The shorter Au–O bond distance is close to that in $Au(OH)_3$ while the active one is close to that in Au_2O_3. In summary, the differences between an active and an inactive Au–O morphology in the pH 4.1 and

10.3 samples include a shorter Au–O bond distance, the presence of a Au . . . Al (Au–O–Al) bonding environment, and a somewhat lower electron density in the inactive catalyst. Though it is not known which one is the main cause of the different activity, it is sure that only a certain form of Au–O morphology can be active. Using terminology from previously proposed synergistic models, only certain Au–oxide interactions can be active; however, the synergistic effect may not be necessary. From the deposition mechanism described in the above section, the active one was found as a consequence of polymeric $Au(OH)_3$ precipitation, whereas the inactive one involved the anchoring of $Au(OH)_3$ via surface hydroxyl groups. This seems to coincide with the precipitation of $Au(OH)_3$ proposed in the $Au/Mg(OH)_2$ prepared from a different deposition procedure, which involves the pH adjustment of precursor solution followed by the addition of support (15). This suggests that polymeric $Au(OH)_3$ precipitate is the morphology that leads to the active phase for supported Au catalysts.

5. CONCLUSION

This study used a deposition procedure including the pH adjustment of the γ-Al_2O_3 suspension, followed by the addition of Au precursor solution and a room-temperature drying of the nonwashed filtered cake. Based on EXAFS analysis, the effect of pH on the Au deposit following our procedure is mainly on the second coordination shell of Au. A surface-anchored $Au(OH)_3$-like deposit was found when the catalyst was prepared at lower pH whereas a polymeric $Au(OH)_3$ deposit was identified at pH higher than 9.5. The polymeric $Au(OH)_3$ deposit leads to a more active catalyst for CO oxidation at 323 K. This suggests that oxidic Au may be the active structure for low-temperature CO oxidation; however, only certain oxidic structures involving the second shell contribution can lead to active supported Au catalysts.

ACKNOWLEDGMENTS

This research was supported by the National Science Council, Taiwan, R.O.C., under Contract NSC86-2214-E-155-005 and NSC86-2113-M-155-001. Dr. Jyh-Fu Lee of SRRC is acknowledged for his timely help in EXAFS experiment as well as for thoughtful discussion.

REFERENCES

1. Haruta, M., Yamada, N., Kobayashi, T., and Iijima, S., *J. Catal.* **115**, 301 (1989).
2. Haruta, M., Tsubota, S., Tessuhiko, T., Kageyama, H., Genet, M. J., and Delmon, B., *J. Catal.* **144**, 175 (1993).
3. Haruta, M., *Catal. Today* **36**, 153 (1997).
4. Haruta, M., *Catal. Surv. Jpn.* **1**, 61 (1997).
5. Bond, G. C., and Thompson, D. T., *Catal. Rev.–Sci. Eng.* **41**, 319 (1999).
6. For example, Everett, D. H., "Basic Principles of Colloid Science," Royal Chem. Soc., London, 1988.
7. Chen, Y.-J., and Yeh, C.-T., *J. Catal.* **200**, 59 (2001).
8. Lin, S. D., Bollinger, M., and Vannice, M. A., *Catal. Lett.* **17**, 245 (1993).
9. Bollinger, M., and Vannice, M. A., *Appl. Catal. B* **8**, 417 (1996).
10. Grunwaldt, J.-D., and Baiker, A., *J. Phys. Chem. B* **103**, 1002 (1999).
11. Clark, E. S., Templeton, D. H., and MacGillavry, C. H., *Acta Crystallogr.* **11**, 284 (1958).
12. Jones, P. G., Rumpel, H., Schwarzmann, E., Sheldrick, G. M., and Paulus, H., *Acta Crystallogr. Sect. B* **35**, 1435 (1979).
13. Baes, C. F., Jr., and Mesmer, R. E., "The Hydrolysis of Cations." Wiley, New York, 1976.
14. Baraj, B., Sastre, A., Merkoci, A., and Martinez, M., *J. Chromatogr. A* **718**, 227 (1995).
15. Cunningham, D. A. H., Vogel, W., Kageyama, H., Tsubota, S., and Haruta, M., *J. Catal.* **177**, 1 (1998).
16. Jones, P. G., and Sheldrick, G. M., *Acta Crystallogr. Part C* **40**, 1776 (1984).
17. Linde, D. R., Ed., "CRC Handbook of Chemistry and Physics," 78th ed., CRC Press, Boca Raton, FL, 1997.
18. Bassi, I. W., Lytle, F. W., and Parravano, G., *J. Catal.* **42**, 139 (1976).
19. Klassen, H., and Hoppe, R., *Naturwissenschaften* **63**, 387 (1976).
20. Torigoe, K., and Esumi, K., *Langmuir* **8**, 59 (1992).
21. Gangopadhayay, A. K., and Chkravorty, A., *J. Chem. Phys.* **35**, 2206 (1961).
22. Schubert, M. M., Hackenberg, S., van Veen, A. C., Muhler, Plzak, V., and Behm, R. J., *J. Catal.* **197**, 113 (2001).
23. Wagner, F. E., Galvagno, S., Milone, C., Visco, A. M., Stievano, L., and Calogero, S., *J. Chem. Soc. Faraday Trans.* **93**, 3403 (1997).
24. Finch, R. M., Hodge, N. A., Hutchings, G. J., Meagher, A., Pankhurst, Q. A., Siddiqui, M. R. H., Wagner, F. E., and Whyman, R., *Phys. Chem. Chem. Phys.* **1**, 485 (1999).
25. Stangland, E. E., Stavens, K. B., Andres, R. P., and Delgass, W. N., *Stud. Surf. Sci. Catal.* **130**, 827 (2000).
26. Puddephatt, R. J., "The Chemistry of Gold," 2nd ed. Elsevier, Amsterdam, 1980.
27. Farges, F., Sharps, J. A., and Brown, G. E., Jr., *Geochim. Cosmochim. Acta* **57**, 1243 (1993).